Research Article

Open Access

Stefan Wachter, Marco Gavagnin, Heinz D. Wanzenboeck*, Mostafa M. Shawrav, Domagoj Belić, Emmerich Bertagnolli

Nitrogen as a carrier gas for regime control in focused electron beam induced deposition

Abstract: This work reports on focused electron beam induced deposition (FEBID) using a custom built gas injection system (GIS) equipped with nitrogen as a gas carrier. We have deposited cobalt from $Co_2(CO)_8$, which is usually achieved by a heated GIS. In contrast to a heated GIS, our strategy allows avoiding problems caused by eventual temperature gradients along the GIS. Moreover, the use of the gas carrier enables a high control over process conditions and consequently the properties of the synthesized nanostructures. Chemical composition and growth rate are investigated by energy dispersive X-ray spectroscopy (EDX) and atomic force microscopy (AFM), respectively. We demonstrate that the N_2 flux is strongly affecting the deposit growth rate without the need of heating the precursor in order to increase its vapour pressure. Particularly, AFM volume estimation of the deposited structures showed that increasing the nitrogen resulted in an enhanced deposition rate. The wide range of achievable precursor fluxes allowed to clearly distinguish between precursor- and electron-limited regime. With the carrier-based GIS an optimized deposition procedure with regards to the desired deposition regime has been enabled.

Keywords: FEBID, carrier gas, cobalt, dicobalt octacarbonyl, gas injection system, GIS, SEM, nitrogen, electron limited regime, precursor limited regime

*Corresponding author: Heinz D. Wanzenboeck: Institute of Solid State Electronics, Vienna University of Technology, Floragasse 7/1, A-1040 Vienna, Austria *e-mail: heinz.wanzenboeck@tuwien.ac.at
Stefan Wachter, Marco Gavagnin, Mostafa M. Shawrav, Domagoj Belić, Emmerich Bertagnolli: Institute of Solid State Electronics, Vienna University of Technology, Floragasse 7/1, A-1040 Vienna, Austria

1 Introduction

The synthesis of ferromagnetic nanostructures has received great attention over the past few years. These structures are usually manufactured by lithographic structuring of a substrate, blanket deposition of the desired magnetic material and a subsequent lift-off process [1,2]. As a successful alternative to this multi-step procedure, focused electron beam induced deposition (FEBID) allows the mask- and resist-less nanofabrication of planar and three dimensional (3D) structures [3]. In FEBID, the focused electron beam (FEB) of a scanning electron microscope (SEM) locally supplies the energy needed to activate the precursor and induce a local chemical vapour deposition process. The direct-write nature of FEBID enables high flexibility in the (three dimensional) design of the deposited objects, avoiding complex and time-consuming multi-step lithography processes [4,5]. This makes FEBID an excellent candidate for research and prototyping applications, such as circuit editing or the design and fabrication of various nanosystems, *e.g.*, in sensing applications as well as data-storage and processing [6–8]. In FEBID a variety of precursors containing magnetic elements is available [3,5]. High purity magnetic materials based on Fe and Co were already synthesized by FEBID using carbonyl (CO) based precursors, for their application in magnetic sensing and logic technologies [8,9]. The choice of these chemicals is driven by the relatively "clean" decomposition path and their high volatility [3]. It has been shown [3, 10, 11] that precursor flow as well as the FEB current are important factors effecting chemical and geometric properties of the deposit. To further enhance the growth rate using CO-based substances, a sufficiently high precursor flux is necessary [12]. For this reason the whole gas injection system (GIS) is often heated up in order to increase the vapour pressure and thereby precursor flux to the deposition area [13]. However, temperature gradients along the delivery system may lead to undesirable re-condensation or deposition of precursor molecules

onto the GIS sidewalls. In this work, we focus on the FEBID of Co from $Co_2(CO)_8$ on Si(100) substrate. Our approach consists of increasing the evaporation rate of precursor by keeping the atmosphere in the reservoir from saturating with precursor by removing the gaseous phase from the reservoir using nitrogen as a carrier gas.

This is expected to increase the flux of precursor molecules impinging on the substrate, enhancing the growth rate while avoiding any heating of precursor reservoir, gas-line or substrate. It is also crucial to find a suitable balance between the electrons supplied by the FEB and the amount of delivered precursor molecules to be decomposed by these electrons. This balance leads to deposition in one of two regimes - the precursor limited regime (PLR) and the electron (beam) limited regime (ELR). When working in the ELR, there is an abundance of precursor molecules, which means the deposition rate is limited by the ability of the electron beam to decompose them. The PLR on the other hand is limited by the amount of precursor available while there is an excess of electrons delivered by the FEB. Here we show how the use of an inert gas carrier allows the fine control of the chosen process regime, highlighting the advantages of ELR and PLR in terms of deposition rates and chemical composition.

2 Methods

The focused electron beam induced deposition (FEBID) was performed in a Zeiss Leo1530VP scanning electron microscope equipped with a custom built gas injection system (GIS) (see Fig.1). This GIS enables injection of evaporated precursor from the precursor reservoir, supported by the carrier gas through a nozzle in close proximity to the substrate. The tip of the nozzle was about 100 μm above the substrate and 95 μm offset laterally, with respect to the impinging spot of the electron beam.

A mass flow controller in the carrier gas line of the GIS enables control over the flux of the carrier gas as main varying parameter. We measured the pressure, both in the GIS line as well as in the SEM chamber. The base pressure of the chamber when no precursor was injected was 3.4×10^{-6} mbar. Nitrogen as a carrier gas was chosen because of its relatively inert properties. Without any carrier gas the precursor flux is limited by the temperature-dependent evaporation rate and the flow resistance of the GIS which resulted in a chamber pressure of $P_{chamber} = 6.2 \times 10^{-6}$ mbar. The GIS was purged through the bypass line (Fig. 1) for roughly 40 min with 5 sccm of N_2. The carrier gas flux values used for the deposition were increased from 0 sccm, *i.e.* deposition without any carrier gas, to a maximum of 0.91 sccm, which still allowed safe operation of our particular system ($P_{chamber} \leq 1 \times 10^{-4}$ mbar). All other parameters, *e.g.*, dwell time, pixel spacing and FEB current, where kept constant. Squares where deposited on Si(100) with a native oxide layer, using a Raith ELPHY Plus pattern generator to precisely guide the beam. The 1 x 1 μm^2 areas were exposed by raster scan, using a pixel spacing of 5 nm and a refresh time between each line of 10 ms, resulting in a deposition time of roughly 3.5 minutes per square. In a separate experiment the FEB current was also varied between 50 pA and 1.64 nA by changing the condenser aperture of the SEM while the flux of carrier gas was kept constant.

After deposition the sample was transferred to a second SEM, a Zeiss NEON 40 EsB CrossBeam system equipped with a 30 mm^2 X-ray detector (EDS 7427) from Oxford Instruments, to perform chemical analysis by energy-dispersive X-ray spectroscopy (EDX) at 5 kV. During the transfer the sample was exposed to air for less than one minute and we expect a slight increase in oxygen content caused by a thin oxidation layer on the surface of the deposit [14]. Topographical analysis was performed by atomic force microscopy (AFM) using a Dimension 3100 system from Veeco/Bruker.
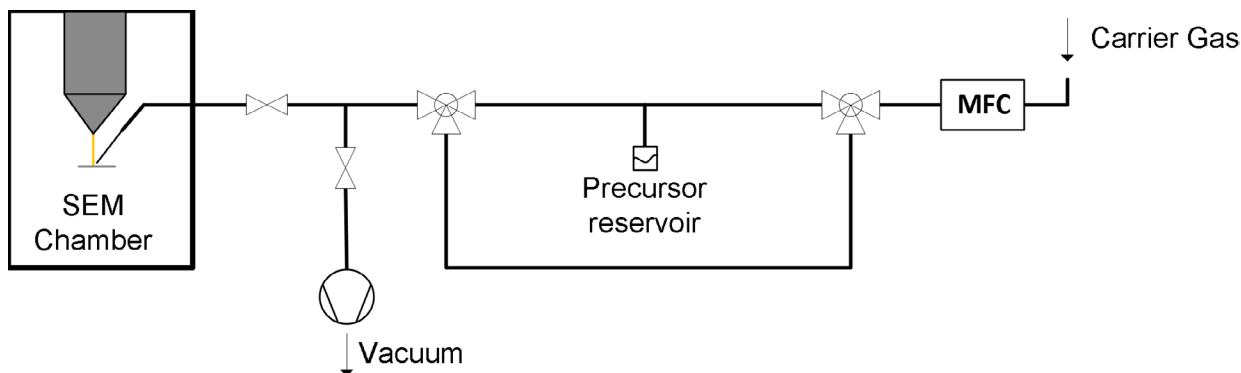

Figure 1: Overview of the gas injection system, comprising of mass flow controller (MFC) to control carrier gas flux, precursor reservoir as well as bypass line and auxiliary vacuum pump. The auxiliary vacuum pump in combination with the bypass line allows efficient precursor purging independent of the SEM chamber.

3 Results

The injection of precursor via a carrier gas flow is an unconventional approach for FEBID. It is not clear whether a precise adjustment of a chamber pressure can be achieved when using a carrier-gas system. For this reason, a systematic investigation of the resulting chamber pressure for each carrier gas flux was performed. The carrier gas flow is determined by a mass flow controller in the carrier gas line. A newly set precursor flux resulted in a new chamber pressure stabilizing within a few minutes. Figure 2 shows an excellent correlation between the set carrier gas flow and the resulting chamber pressure. This demonstrates that our setup enables an accurate control over the flux of the carrier gas as main varying parameter (see Figure 2). However, a higher chamber pressure does not necessarily imply a higher flux of precursor. This cannot be determined by a measurement of chamber pressure alone but only by actual deposition and subsequent investigation of the structures. To prove the difference in precursor fluxes by varying the nitrogen flux, $1 \times 1 \ \mu m^2$ Co structures were synthesized. An SEM micrograph and corresponding AFM 3D plot of such a Co square deposit are shown in Fig. 3a and b. The self-built GIS is not only equipped with a mass flow controller for the gas carrier injection, but also provides the possibility of purging the system with a supplementary bypass line as shown in Figure 1. Furthermore, the GIS can be evacuated through a secondary vacuum line (bypass), positioned before the SEM chamber. This avoids multiple purging cycles conventionally executed directly via the SEM vacuum system, and thereby limits the contamination in the chamber. AFM profile analysis of the deposited structures are shown in Figure 3c. It is widely acknowledged that the primary electrons (PE) from the beam are not the main reason for the decomposition of the precursor. Inelastic scattering with the structure or substrate will produce secondary electrons (SE1). These SE1 are primarily responsible for the growth of the main structures themselves [9,14]. Elastic scattering of the PE on the structure itself and on the substrate gives rise to the so called forward (FSE) and back scattered electrons (BSE), respectively. These BSE will themselves cause secondary electrons (SE2) by inelastic scattering with the substrate atoms. These SE2 and BSE are responsible for the formation of a so called halo layer, a thin, circular deposit around the actual structure itself [15]. In close proximity to the actual structure the thickness of the halo layer gradually increases, forming a smooth transition instead of a sharp corner at the base of the structure (Figures 3c, 3d). We assume this is due to a combination of the aforementioned secondary electrons, as well as a not infinitely sharp beam profile. Furthermore, it is clearly visible that halo layer immediately around the structures is not symmetrical. The side facing the nozzle from which the precursor flux is originating receives more precursor [12], which leads to a comparatively higher deposition at the base of the deposit. This asymmetry, while only slightly visible without carrier gas, becomes more pronounced at higher fluxes. We assume this is due to a slower replenishment of precursor on the side pointing away from the nozzle because the precursor flux is shadowed by the structure itself [12]. It is clear that a close attention must be paid to this phenomenon, especially in a case where functional structures are to be synthesized in close proximity to each other [9, 16]. The AFM profiles also show a stabilization of the height of the deposits with higher fluxes indicating a saturation of the growth rates with higher fluxes.

A more detailed observation on this saturation of the growth rate is given by the volume variation of the deposits with the increasing nitrogen flux (Figure 4a). The deposited volume increases linearly with low fluxes, while stabilizing at higher values (above 0.40 sccm), indicating a transition from precursor-limited regime (PLR) to the electron-limited regime (ELR). Since the transition from the PLR to ELR was not accurately distinguishable in the volume trends by only varying the carrier gas fluxes, we also varied the beam current at a steady flux. The flux we have chosen for this variation in the beam current was 0.38 sccm, which was the suspected transition point. This 'point of intersection' is highlighted in Figure 4 and Figure 5. For the variation of the beam current, we deposited $1 \times 1 \ \mu m^2$ square structures at the aforementioned flux and a constant exposure time. At low beam current values,
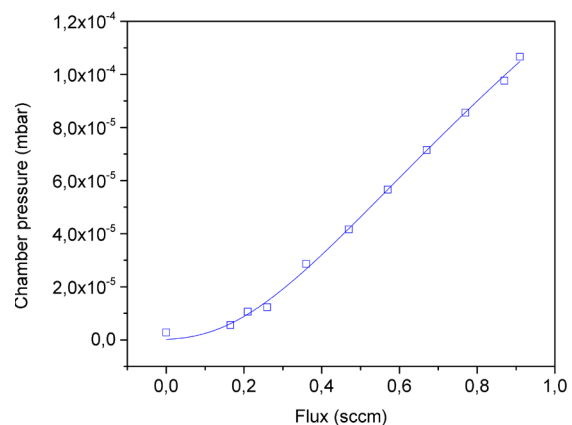

Figure 2: Pressure in the SEM chamber at different values (0 sccm – 0.91 sccm) of nitrogen carrier gas injected in combination with the precursor. The base pressure of the system prior to injection of any gas was $P_{chamber} = 3.4 \times 10^{-6}$ mbar.
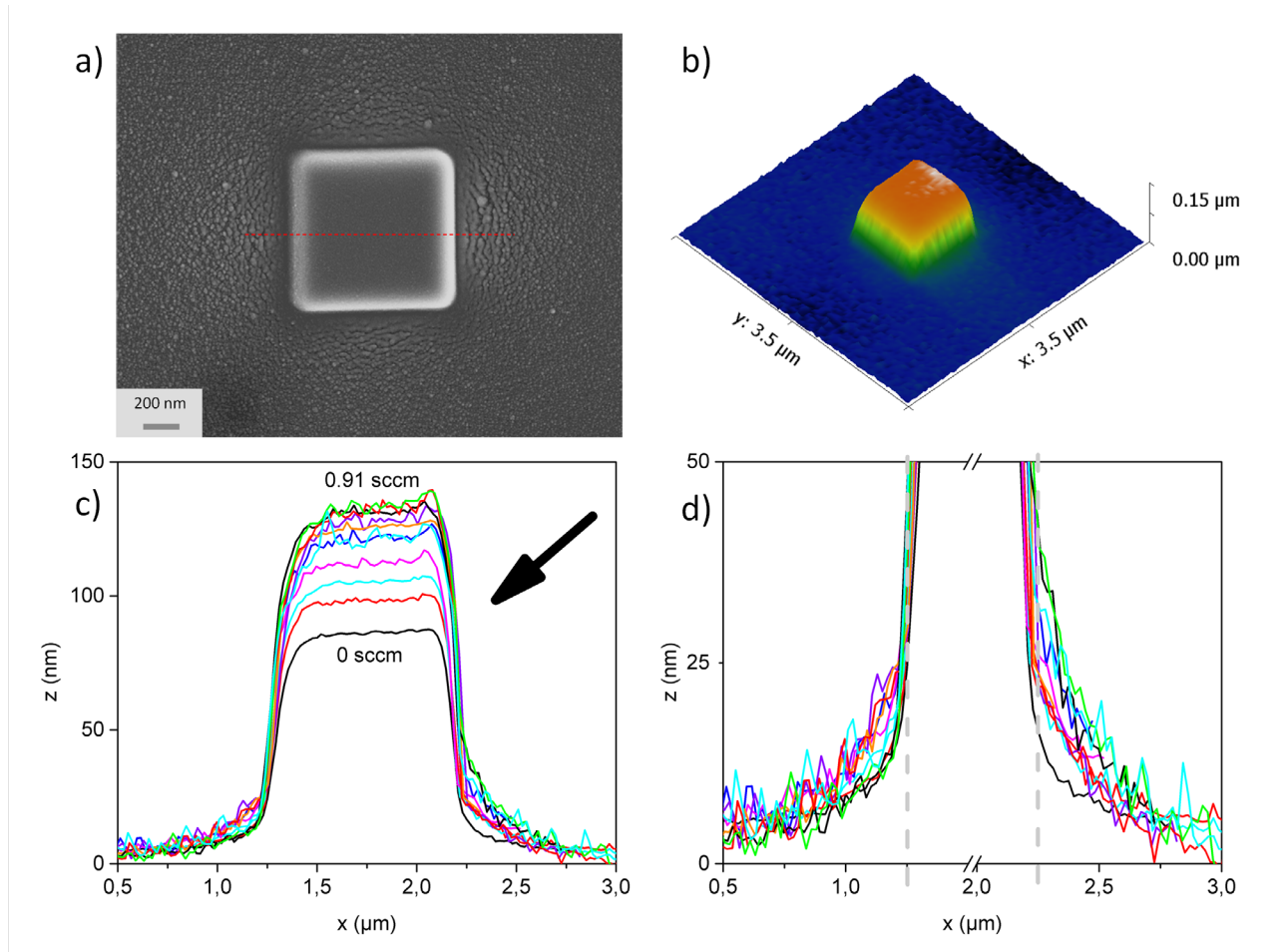
Figure 3: a,b) SEM micrograph and corresponding AFM 3D view of a 1 x 1 μm² square deposited at a nitrogen flux of 0.87 sccm. c) Profile of the deposits synthesized at different fluxes from 0 sccm to 0.91 sccm along the dashed red line in the SEM micrograph. The arrow on the right hand side of the deposit indicates the position of the GIS-nozzle. d) Close up of the base of the structure, grey dashed lines indicate vertical sidewalls of the structure

an ELR is established since a linear trend of the volume growth is observed (Fig. 5a). Further increase of the beam current to values > 0.5 nA stabilize the deposition rate to a maximum, meaning that the process is in a PLR. These measurements indicate that at the investigated flux value of 0.38 sccm and 1 nA of beam current, deposition is occurring in the PLR and the growth rate can be enhanced only by increasing the precursor flux. Therefore, the transition point must be at higher fluxes, namely between 0.40 sccm and 0.45 sccm at I_{beam} = 1 nA.

Another crucial characteristic of the deposited structures is their chemical composition. Both, electrical applications as well as those based on magnetism require a high metal content. In Figure 4c the EDX spectrum of the Co square deposited at highest nitrogen flux (0.91 sccm) is shown. The main contaminants detected by EDX are O and C, while no traces of nitrogen have been detected. Particularly, O and C may both originate from

residual precursor fragments that are incorporated in the structures and [17] from residual gas (RG) present in the SEM chamber. The RG in the high vacuum chambers is mainly composed of H_2, He, O_2, N_2, H_2O and C-containing species. In particular, these last carbonaceous species are incorporated in the structure during the FEBID process [18]. Furthermore, the parasitical deposition of C-contaminants can also occur during EDX analysis leading to an overestimation of the carbon content. Increasing the nitrogen flux, carbon remained largely constant, while the amount of oxygen increased significantly (Figure 4b). Particularly the increase in oxygen content with increasing flux is a symptom of the decreasing purity due to the incorporation of precursor that has not been fully decomposed by the electron beam (ELR) [10,11,17]. This assumption is supported by the fact that at higher beam currents oxygen contamination is decreasing significantly at constant volume (Fig. 5b).
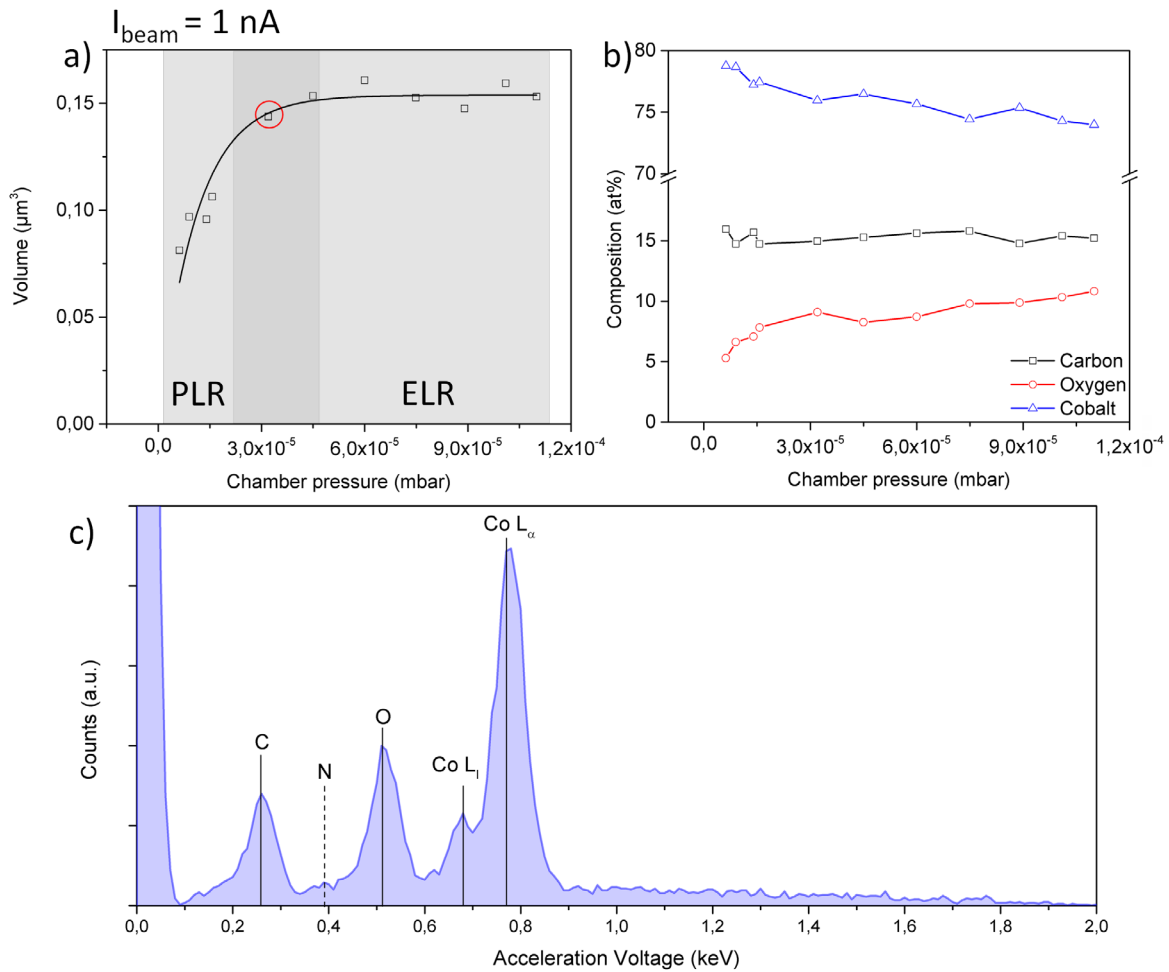
Figure 4: a) Deposited volume and b) chemical composition trends of the structures deposited at different fluxes of nitrogen and a beam current of I_{beam} = 1 nA. PLR and ELR have been observed at low and high fluxes of nitrogen, respectively. The darker grey area indicates a transition zone between the two regimes. Further experiments were performed at 0.38 sccm (red circle in a)) in order to correctly identify the transition point. c) shows a full EDX spectrum of a deposit created at a flux of 0.87 sccm, confirming the absence of nitrogen in the deposits.
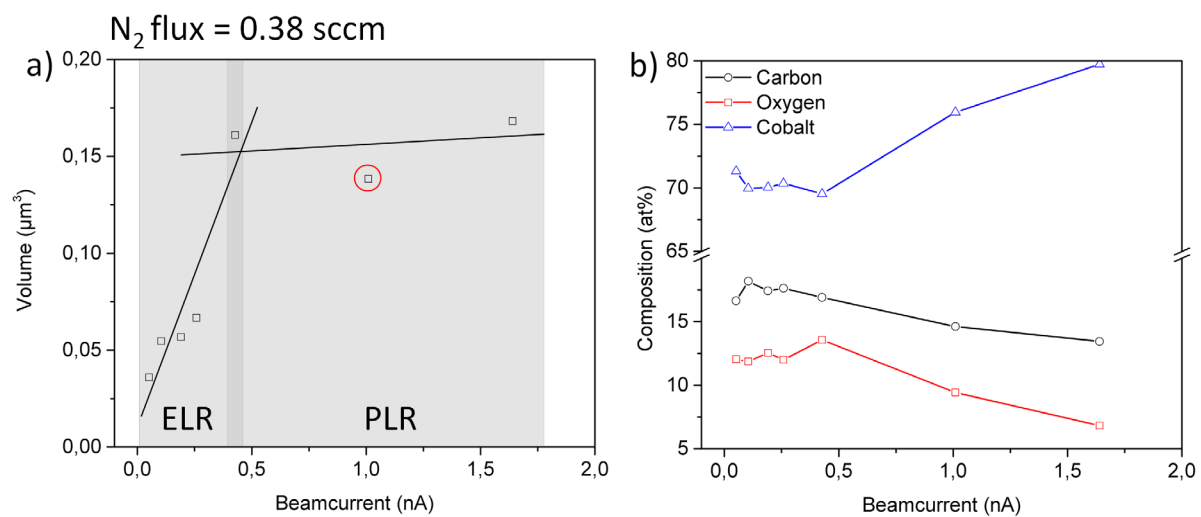

Figure 5: Deposited volume and chemical composition of the structures with constant flux of 0.38 sccm and varying beam current. Electron- and precursor limited regime are indicated in the figure. The highlighted point (red circle in a)) of intersection with previous experiments is clearly situated in the PLR.

In this condition the FEB supplies enough electrons to better decompose the large amount of precursor molecules available - a transition to the PLR. Due to the planar structure of our deposits thermal effects caused by e-beam heating are assumed to be negligible, since most e-beam heating effects are reported in non-planar, tip-like structures offering a greatly decreased heat conducting path and at significantly higher FEB currents [19]. An important result of this work is the accurate definition of the transition from PLR to ELR. This provides a key-advantage because while PLR deposits are typically of high purity but slow to deposit, structures synthesized in the ELR are usually characterized by fast deposition and decreased purity [10,17,20]. Both, a high rate of deposition reducing the processing time as well as a high purity are desirable. This point of transition can be regarded as a 'sweet spot' of maximum deposition rate without an unnecessary sacrifice of purity.

4 Conclusion

We have demonstrated the feasibility of using a carrier gas as a precursor flux enhancer in FEBID for low vapour pressure precursors such as $Co_2(CO)_8$ at room temperature. This increase in precursor flux allows increased and more controlled deposition rate by varying the working point with regards to the amount of available precursor gas, without the disadvantages brought on by the usually employed heating of the precursor. The precise control of gas supply is fundamental to tune the process regime for the desired application. For depositions where purity is crucial, the PLR should be chosen, although the deposition rate decreases. When purity is not the main focus, deposition rate can be improved by shifting the deposition further towards the ELR until the transition point is met. Beyond this point the deposition rate saturates and any further increase in the precursor supply unnecessarily contaminates the structures. Furthermore, this simplifies additional research in the topic of FEBID, since an accurate control of deposition regime is enabled by our strategy.

The presented method for enhancing the deposition rate by the use of a carrier gas is widely applied in CVD processes, *e.g.*, thermal or plasma-activated. Hence, we believe that our strategy is potentially suitable for other classes of precursors characterized by a relatively low vapour pressure.

In future work, other types of reactive carrier gases will be examined, which are expected to influence not only the deposition rate, but also the chemistry of the final deposit.

References

[1] Niemier M., Bernstein G., Csaba G., Dingler A., Hu X., Kurtz S., Liu S., Nahas J., Porod W., Siddiq M., et al.,Nanomagnet logic: progress toward system-level integration, J Phys Condens Matter, 2011,23,493202.
[2] Martin J., Nogues J., Liu K., Vicent J., Schuller I.K.,Ordered magnetic nanostructures: fabrication and properties, J Magn Magn Mater, 2003,256,449–501.
[3] Utke I., Hoffmann P., Melngailis J.,Gas-assisted focused electron beam and ion beam processing and fabrication, J Vac Sci Technol, B, 2008,26,1197–276.
[4] Hoffmann P., Utke I., Cicoira F., Dwir B., Leifer K., Kapon E., Doppelt P.,Focused Electron Beam Induced Deposition of Gold and Rhodium. MRS Proceedings, vol. 624, 2000, p. 171.
[5] Botman A., Mulders J., Hagen C.,Creating pure nanostructures from electron-beam-induced deposition using purification techniques: a technology perspective, Nanotechnology, 2009,20,372001.
[6] Chappert C., Fert A., Van Dau F.N.,The emergence of spin electronics in data storage, Nat Mat, 2007,6,813–23.
[7] Allwood D.A., Xiong G., Faulkner C., Atkinson D., Petit D., Cowburn R.,Magnetic domain-wall logic, Science, 2005,309,1688–92.
[8] Serrano-Ramón L., Córdoba R., Rodríguez L.A., Magén C., Snoeck E., Gatel C., Serrano I., Ibarra M.R., De Teresa J.M.,Ultrasmall functional ferromagnetic nanostructures grown by focused electron-beam-induced deposition, ACS Nano, 2011,5,7781–7.
[9] Gavagnin M., Wanzenboeck H.D., Belic D., Bertagnolli E.,Synthesis of Individually Tuned Nanomagnets for Nanomagnet Logic by Direct Write Focused Electron Beam Induced Deposition, ACS Nano, 2012,7,777–84.
[10] Van Dorp W., Hagen C.,A critical literature review of focused electron beam induced deposition, J Appl Phys, 2008,104,081301.
[11] Huth M., Porrati F., Schwalb C., Winhold M., Sachser R., Dukic M., Adams J., Fantner G.,Focused electron beam induced deposition: A perspective, Beilstein J Nanotechnol , 2012,3,597–619.
[12] Friedli V., Utke I.,Optimized molecule supply from nozzle-based gas injection systems for focused electron-and ion-beam induced deposition and etching: simulation and experiment, J Phys D: Appl Phys, 2009,42,125305.
[13] Lau Y., Chee P., Thong J., Ng V.,Properties and applications of cobalt-based material produced by electron-beam-induced deposition, J Vac Sci Technol, A, 2002,20,1295–302.
[14] Gavagnin M., Wanzenboeck H.D., Belic D., Shawrav M.M., Persson A., Gunnarsson K., Svedlindh P., Bertagnolli E.,Magnetic force microscopy study of shape engineered FEBID iron nanostructures, Phys Status Solidi A, 2013.
[15] Fowlkes J.D., Randolph S.J., Rack P.D.,Growth and simulation of high-aspect ratio nanopillars by primary and secondary electron-induced deposition, J Vac Sci Technol, B, 2005,23,2825–32.
[16] Nikulina E., Idigoras O., Porro J., Vavassori P., Chuvilin A., Berger A.,Origin and control of magnetic exchange coupling in between focused electron beam deposited cobalt nanostructures, Appl Phys Lett, 2013,103,123112.

[17] Hoyle P., Ogasawara M., Cleaver J., Ahmed H.,Electrical resistance of electron beam induced deposits from tungsten hexacarbonyl, Appl Phys Lett, 1993,62,3043–5.

[18] Wanzenboeck H., Roediger P., Hochleitner G., Bertagnolli E., Buehler W.,Novel method for cleaning a vacuum chamber from hydrocarbon contamination, J Vac Sci Technol, A, 2010,28,1413.

[19] Utke I., Bret T., Laub D., Buffat P., Scandella L., Hoffmann P.,Thermal effects during focused electron beam induced

deposition of nanocomposite magnetic-cobalt-containing tips, Microelectron Eng, 2004,73,553–8.

[20] Córdoba R., Fernández-Pacheco R., Fernández-Pacheco A., Gloter A., Magén C., Stéphan O., Ibarra M.R., De Teresa J.M.,Nanoscale chemical and structural study of Co-based FEBID structures by STEM-EELS and HRTEM, Nanoscale Res Lett, 2011,6,1–6.